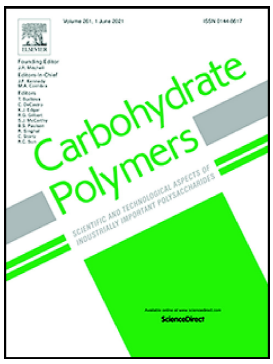

Comparison of the properties of turmeric starch-dioscin-curcumin nanocarriers prepared by antisolvent co-precipitation and antisolvent precipitation

Wenqing Zhu, Xinyan Bai, Wenbo Du, Lingyu Li, Marie-Laure Fauconnier, Aurore Richel, Hongjing Dong, Zhenjia Zheng

PII: S0144-8617(25)00044-X

DOI: https://doi.org/10.1016/j.carbpol.2025.123263

Reference: CARP 123263

To appear in: *Carbohydrate Polymers*

Received date: 14 October 2024

Revised date: 20 December 2024

Accepted date: 10 January 2025

Please cite this article as: W. Zhu, X. Bai, W. Du, et al., Comparison of the properties of turmeric starch-dioscin-curcumin nanocarriers prepared by antisolvent co-precipitation and antisolvent precipitation, *Carbohydrate Polymers* (2024), https://doi.org/10.1016/j.carbpol.2025.123263

Comparison of the properties of turmeric starch-dioscin-curcumin nanocarriers prepared by antisolvent co-precipitation and antisolvent precipitation

Wenqing Zhu[a,b], Xinyan Bai[a,b], Wenbo Du[c], Lingyu Li[a], Marie-Laure Fauconnier[b], Aurore Richel[d], Hongjing Dong[e], Zhenjia Zheng[a,*]

[a] Key Laboratory of Food Nutrition and Healthy in Universities of Shandong, College of Food Science and Engineering, Shandong Agricultural University, 61 Daizong Street, Tai'an 271018, Shandong, China

[b] Laboratory of Chemistry of Natural Molecules, Gembloux Agro-Bio Tech, University of Liège, Passage des déportés 2, B-5030, Gembloux, Belgium

[c] Jilin Province Product Quality Supervision and Inspection Institute, 2699 Yiju Road, Changchun 130103, Jilin, China

[d] Laboratory of Biomass and Green Technologies, Gembloux Agro-Bio Tech, University of Liège, Passage des déportés 2, B-5030, Gembloux, Belgium

[e] Shandong Analysis and Test Center, Qilu University of Technology (Shandong Academy of Sciences), Jinan 250014, Shandong, China

[*] Corresponding author: College of Food Science and Engineering, Shandong Agricultural University, 61 Daizong Street, Tai'an 271018, Shandong, China. Email: pengyou-jia@163.com

Abstract: In this study, two modified turmeric starch-dioscin-curcumin nanocarriers were synthesized by antisolvent co-precipitation (ASCP) and antisolvent precipitation (ASP) methods, with dioscin serving as a natural surfactant. Subsequently, the structural

characteristics, physical stability, and curcumin sustained release properties of nanocarriers were comprehensively characterized. The results indicated that both modified nanocarriers exhibited similar morphology and functional groups, along with enhanced physical stability and storage stability. Both ASCP and ASP methods reduced the particle size of nanocarriers while enhancing encapsulation efficiency and loading capacity. Notably, the nanocarrier prepared using the ASCP method exhibited the smallest particle size (260.50 ± 9.01 nm), the highest encapsulation efficiency (59.06 ± 1.73 %), and the greatest loading capacity (7.18 ± 0.21 μg/mg). Additionally, the release rate and bioavailability of ASCP-TS-CUR were approximately 23 and 20 times higher than free curcumin, respectively. These findings support the potential of dioscin-modified starch nanocarriers for the effective delivery of hydrophobic compounds, and the ASCP method was proved to have better modification effects, providing a novel green strategy for the construction of delivery systems.

Keywords: Starch, curcumin, dioscin, antisolvent co-precipitation, antisolvent precipitation, structural characterization, *in vitro* release

1. Introduction

Curcumin, an essential component of turmeric, is a hydrophobic polyphenol with various biological functions such as antioxidant, anti-inflammatory, and anti-cancer (Ferguson et al., 2021). However, its poor water solubility (11 ng/mL), poor stability, and low bioavailability (Xiang et al., 2020) limit its application in the food and medical industries. To address these challenges, researchers have developed a variety of nanodelivery systems, such as nanoemulsions (Marefati et al., 2017; Araiza-Calahorra et al., 2019), solid lipid nanocarriers

(Karaca et al., 2025), and nanoparticles based on polysaccharides and proteins (Zou et al., 2016) have been used to encapsulate curcumin to enhance its stability and bioavailability. Among them, starch-based nanoparticles showed great advantages due to their safety, non-toxicity, good biocompatibility, and low cost, and are widely used for the delivery of curcumin (Du et al., 2023). For instance, banana starch nanoparticles (Acevedo-Guevara et al., 2018) and corn starch nanoparticles (Zhong et al., 2024) have been successfully used to deliver curcumin.

We aim to explore a novel starch-based carrier to protect and deliver curcumin. Turmeric contains a high content of starch, about 40%, which is often neglected when curcumin is extracted (Kuttigounder et al., 2011), resulting in a waste of starch resources. Furthermore, studies have shown that turmeric starch is non-toxic and well tolerated at high doses (Rasmi et al., 2024), and therefore can be developed and utilized as a safe by-product. However, research on the development and utilization of turmeric starch remains relatively scarce. Considering this, turmeric starch has the potential to be developed as a novel starch-based nanocarrier to protect curcumin from environmental degradation, improve its stability, achieve persistent release in the gastrointestinal tract, and enhance its bioavailability. Notably, native starch granules usually have a large size and a wide distribution, limiting their application as a stable carrier material (Li et al., 2016a). To solve this problem, surfactants can be used for modification, which can decrease interfacial tension and aggregation, thereby reducing particle size and constructing starch nanoparticles with stable performance and controllable particle size (Ye et al., 2017). At present, commercial synthetic surfactants (such as Tween 80 and Span 80) (Li et al., 2016a) may bring potential safety hazards despite their high efficiency and low cost

(Zargar et al., 2024). In recent years, utilizing natural surfactants to enhance product performance has become an important trend due to their natural origin, safety, and environmental sustainability. Plant saponins are an option used as a natural surfactant in the food industry (Henao-Ardila et al., 2024). Currently, there are studies using tea saponins and quillaja saponins as natural surfactants to stabilize polymer carriers (Liu et al., 2022; Doost et al., 2019). Apart from them, dioscin, a common plant steroidal saponin (Tao et al., 2018), has good amphiphilic properties, high surface activity, and possesses a variety of biological activities, such as antibacterial, anti-inflammatory, anti-tumor, immune-regulation, and antiviral effects (Bandopadhyay et al., 2022), which may make it a promising natural surfactant (Liao et al., 2021). However, research on the potential application of dioscin as a natural surfactant is lacking. Antisolvent co-precipitation (ASCP) and antisolvent precipitation (ASP) are effective methods for preparing nanoparticles and delivering active substances (Chen et al., 2021; Sun et al., 2016). The difference between ASCP and ASP methods is due to the sequence of component mixing, and the different sequences may influence the interaction forces between molecules and subsequently impact encapsulation performance (Yang et al., 2018). Therefore, adjusting the mixing sequence of components is of great significance for improving the performance of delivery systems (Blanco et al., 2015). Nevertheless, there is no existing research on the performance comparison of starch-based nanocarriers prepared using ASCP and ASP methods.

We hypothesized that dioscin can be used as a natural surfactant to reduce the particle size of starch nanocarriers and improve loading performance, while different blending sequences of natural surfactants may also affect the modification effect. To prove our hypothesis, in this study,

dioscin was used to modify curcumin-loaded starch nanocarriers, and then two modified turmeric starch-dioscin-curcumin nanocarriers were synthesized based on different blending sequences of dioscin. Subsequently, the structural characteristics, physical stability, and curcumin release properties of nanocarriers were compared to investigate the modification effects of ASCP and ASP methods. Our research aims to develop a green and novel curcumin nanodelivery system based on natural components and to screen the optimal method for preparing high-performance nanocarriers, which will provide a new strategy for better designing delivery systems for hydrophobic active substances while providing new insights into the high-value utilization of turmeric resources.

2. Materials and methods

2.1. Materials and chemicals

Turmeric was purchased from Anqing Letu Trading Co., Ltd. (Guangxi, China). Curcumin (purity ≥ 99.82 %) and dioscin (purity ≥ 99.67 %) were purchased from Chengdu Munster Bio-Technology Co., Ltd. (Chengdu, China). Simulated saliva, gastric, and intestinal fluids were obtained from Shanghai Yuanye Bio-Technology Co., Ltd. (Shanghai, China). All other chemicals and reagents were of analytical purity.

2.2. Extraction of turmeric starch

Turmeric starch was extracted referring to the method described by Argel-Pérez et al. (2023), with some modifications. Briefly, cleaned fresh turmeric rhizomes were crushed and soaked in 0.3 % NaOH solution for 2 h. The suspension was ground for 3 minutes using a

grinder (SY-8619, Hefei, China) operating at maximum power (1500 W). The ground material was then filtered with a filter cloth (100-mesh), and the remaining solids in the filter cloth were ground in the grinder with added water and filtered again. This process was repeated three times. The slurry passed through the filter cloth was collected and centrifuged at 4000 rpm for 20 min. After discarding the supernatant, the precipitate was washed several times with absolute ethanol and deionized water, and filtered with a 200-mesh filter cloth. Finally, the slurry was centrifuged again, and the precipitate was collected and dried in a drying oven at 45 °C for 12 h to obtain turmeric starch (TS). Moreover, the chemical composition, molecular weight, amylose and amylopectin content, Fourier transform infrared (FITR) spectroscopy, X-ray diffraction (XRD), scanning electron microscopy (SEM), as well as solubility and swelling power of TS were determined (**Text S1** and **Text S2** for details).

2.3. Preparation of turmeric starch-dioscin-curcumin nanocarriers

Referring to the previous method (Liu et al., 2022), with some modifications. Two methods, ASCP and ASP, were utilized to prepare turmeric starch-dioscin-curcumin nanocarriers. The detailed flowchart is shown in **Fig. 1**.

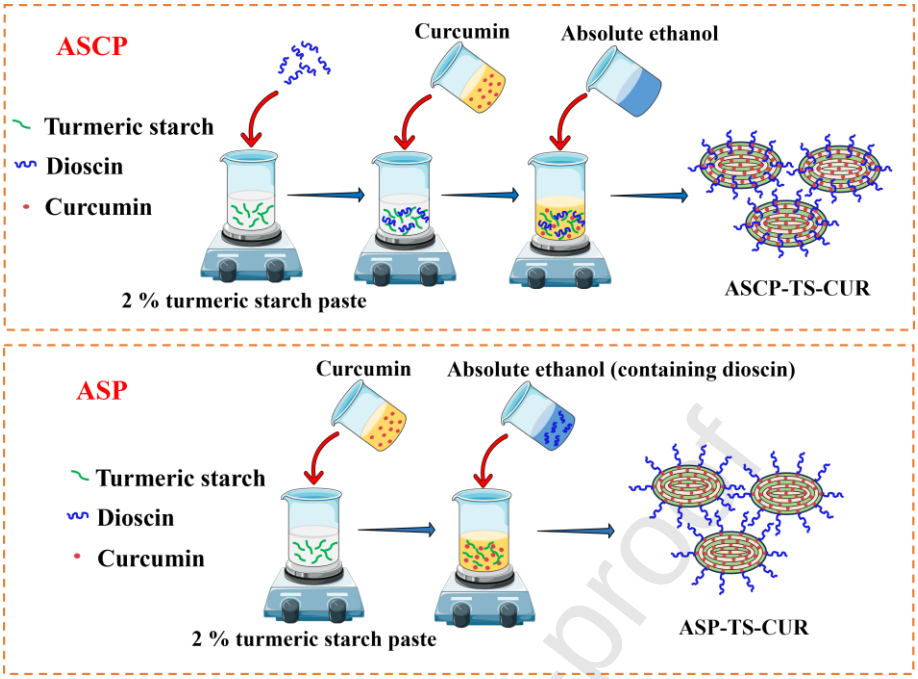

Fig. 1. Flow chart of preparation of turmeric starch-dioscin-curcumin nanocarriers by antisolvent co-precipitation (ASCP) and antisolvent precipitation (ASP) methods.

To prepare turmeric starch-dioscin-curcumin nanocarriers using the ASCP method, firstly a 2.0 % (*w/v*) TS suspension was prepared and gelatinized under magnetic stirring for 30 min at 90 °C. Dioscin (1.5 % (*w/w*) of starch) was then gradually added to the starch paste and stirred at 700 rpm for 30 min. Next, curcumin-absolute ethanol solution with a concentration of 1.0 mg/mL was gradually dripped into the starch-dioscin mixture solution, followed by stirring at 700 rpm at room temperature (RT) for 1 h. Subsequently, absolute ethanol was slowly dripped into the starch-dioscin-curcumin mixture solution, which was continuously stirred for 30 min, followed by starch retrogradation at 4 °C for 24 h. The mixing system was centrifuged (4000 rpm, 10 min), and the precipitate was washed three times with absolute ethanol. Finally, the

precipitate was freeze-dried for 48 h to obtain the turmeric starch-dioscin-curcumin nanocarrier prepared by the ASCP method, which was designated as ASCP-TS-CUR.

To prepare turmeric starch-dioscin-curcumin nanocarriers using the ASP method, firstly a 2.0 % (*w/v*) TS suspension was prepared and gelatinized under magnetic stirring for 30 min at 90 °C. Curcumin-absolute ethanol solution with a concentration of 1.0 mg/mL was gradually added to the starch paste and stirred at 700 rpm for 1 h. Subsequently, absolute ethanol containing dioscin (1.5 % (*w/w*) of starch) was slowly dripped into the starch-curcumin mixture solution and continuously stirred for 30 min, followed by starch retrogradation at 4 °C for 24 h. The mixture system was centrifuged (4000 rpm, 10 min), and the precipitate was washed three times with absolute ethanol. Finally, the precipitate was freeze-dried for 48 h to obtain the turmeric starch-dioscin-curcumin nanocarrier prepared by the ASP method, which was designated as ASP-TS-CUR.

The curcumin-loaded turmeric starch nanocarriers (none dioscin) were also fabricated using the ASP method. Briefly, the turmeric starch paste was blended with the curcumin-absolute ethanol solution, followed by a slow injection of absolute ethanol into the mixture of starch-curcumin. The remaining processes were the same as the ASP method. The nanocarriers prepared by the ASP method without dioscin were referred to as turmeric starch-curcumin nanocarriers, designated as TS-CUR. Similarly, the hollow starch nanocarriers containing neither dioscin nor curcumin were prepared by the ASP method and named TSNC.

2.4. Characterization of nanocarriers

2.4.1. Encapsulation efficiency (EE) and loading capacity (LC)

The determination of EE and LC was carried out using the method described by Acevedo-Guevara et al. (2018). In brief, curcumin from samples was extracted using absolute ethanol under ultrasonic crushing for 20 min, then centrifuged at 4000 rpm for 10 min. After the supernatant was diluted to the appropriate concentration, it was measured at 420 nm using a microplate reader (BioTek Epoch 2, BioTek Instruments, Inc, USA). The curcumin content was calculated based on the standard curve equation of curcumin ($y = 0.0824x + 0.0698$, $R^2 = 0.9969$). The EE and LC were calculated according to Eq. (1) and Eq. (2):

$$EE\ (\%) = \frac{Weight\ of\ encapsulated\ curcumin}{Total\ weight\ of\ curcumin} \times 100 \quad (1)$$

$$LC\ (\mu g/mg) = \frac{Weight\ of\ encapsulated\ curcumin}{Weight\ of\ nanocarriers} \quad (2)$$

2.4.2. Particle size and zeta potential

The particle size, polydispersity index (PDI), and zeta potential were determined using a NS-90Z nanoparticle size and potential analyzer (Omec Instrument Co., Ltd., Zhuhai, China) at 25 °C. The measurement conditions were a sample concentration of 1.0 mg/mL, a scattering angle of 90°, and a refractive index of 1.52 and 1.33 for starch and water, respectively (Guo et al., 2015).

2.4.3. FTIR analysis

The Nicolet iS10 FTIR spectrometer (Thermo Fisher Scientific Inc., Massachusetts, USA) was used for FTIR analysis. Approximately 3.0 mg of sample powders were directly placed on the sample holder and scanned in the wavenumber range of 4000 to 400 cm^{-1}, with a resolution of 4 cm^{-1} and 64 scans (Ye et al., 2019).

2.4.4. Fluorescence spectroscopy analysis

The binding of curcumin to starch was determined using a fluorescence spectrophotometer (Lumina, Thermo Fisher Scientific, Massachusetts, USA) according to the method described by Liang et al. (2023). The emission spectrum was measured in the range of 450 to 800 nm, with an excitation wavelength of 420 nm, a scanning speed of 300 nm/min, and excitation and emission slits of 5 nm.

2.4.5. XRD analysis

Referring to the previous study by Zhi et al. (2021), the crystalline phase of samples was characterized using XRD analysis. The measurement was carried out on an X-ray diffractometer (EMPYREAN, Malvern Panaco Instruments Ltd., Malvern, UK) equipped with a Cu-Kα radiation source at a current of 40 mA and an accelerating voltage of 40 kV. The scanning range of 2θ was 5° to 60°, and the scanning speed was 4°/min.

2.4.6. SEM analysis

Samples were uniformly glued onto the observation stage of a scanning electron microscope (SUPRATM 55, Zeiss, Germany), and next coated with gold in a vacuum environment. The acceleration voltage was 5 kV, and observations were conducted at magnifications of 2000× and 5000× (Du et al., 2023).

2.4.7. Transmission electron microscopy (TEM) analysis

The microstructure of samples was observed by a TEM (Talos F200X G2, FEI Co., MA, USA). The fresh sample solutions were dropped onto the copper mesh, then air-dried and observed at an acceleration voltage of 100 kV.

2.4.8. Thermogravimetric analysis (TGA)

Thermogravimetric analysis of samples was conducted using a D-09123 thermogravimetric analyzer (Mettler Toledo Instruments Ltd., Zurich, Switzerland). Sample powders were heated from 25 °C to 600 °C at a heating rate of 10 °C/min. Nitrogen was used as a protective gas (Zhi et al., 2021).

2.4.9. Differential scanning calorimetry (DSC) analysis

The thermal transition characteristics of samples were measured using a differential scanning calorimetric analyzer (TGA/DSC 3^{+}, Mettler Toledo Instruments Ltd., Zurich, Switzerland) as reported previously (Li et al., 2016b). Sample powders (about 2.5 mg) were mixed with three times its mass of distilled water, then sealed in a crucible and equilibrated under a nitrogen environment for 1 h. The measurement was set as temperature 30 °C to 250 °C, heating rate 10 °C/min, and nitrogen flow rate 40 mL/min.

2.4.10. Rheological analysis

The composite nanocarrier mixture solution after the regeneration step described in section 2.3 was used for the rheological measurement. Before the measurement, the sample solutions were mixed thoroughly to ensure homogeneity. The variation of storage modulus (G′) and loss modulus (G″) of the samples with angular frequency were measured using a MCR102 Modular Intelligent Rheometer (Anton Paar Instruments Co. Ltd., Austria). In the frequency sweep determination, the strain was 0.5 %, and the angular frequency range was 0.1–100 rad/s.

2.5. Physical stability evaluation

2.5.1. Temperature stability

Nanocarrier dispersions were placed in a water bath for 1 h at different temperatures (30,

40, 50, 60, 70, 80, and 90 °C). The particle size, PDI, zeta potential, and curcumin retention rate were determined after the samples were cooled to RT (Song et al., 2021).

2.5.2. Ion stability

The nanocarrier dispersions were incubated in NaCl solutions with different concentrations (50, 100, 150, 200, and 250 mmol/L) and stored at 4 °C for 24 h. The particle size, PDI, zeta potential, and curcumin retention rate were then measured (Wang et al., 2021).

2.5.3. pH stability

The pH of nanocarrier dispersions was regulated to 2, 3, 4, 5, 6, 7, and 8, then stabilized at 4 °C for 24 h. The particle size, PDI, zeta potential, and curcumin retention rate were then determined (Song et al., 2021).

2.5.4. Storage stability

To assess the storage stability of nanocarrier dispersions, fresh sample solutions were stored at either 4 °C or RT for 28 days in the dark, and 0.02 % (*w/v*) sodium azide was added to inhibit microbial growth. The particle size, PDI, zeta potential, and curcumin retention rate of samples were recorded every 7 days.

2.6. In vitro release and bioavailability of curcumin in nanocarriers

The *in vitro* digestive properties and bioavailability of curcumin were studied through simulated digestive system as reported previously (Han et al., 2023). The simulated system was comprised of three stages: Oral stage, gastric stage, and intestinal stage.

2.6.1. Oral stage

Simulated saliva fluid (SSF) was maintained at 37 °C. 50 mL of sample solutions was

mixed with 50 mL of SSF and shaken in a 37 °C shaker for 2 min. Samples were then collected at 0, 1, and 2 min for measurement.

2.6.2. Gastric stage

After the oral digestion, 50 mL of oral phase samples were mixed with 50 mL of simulated gastric fluid (SGF). The pH of the mixture was then regulated to 2.0 and shaken on a shaking table for 2 h (100 rpm, 37 °C). Samples were then collected for measurement at 0, 30, 60, 90, and 120 min.

2.6.3. Intestinal stage

After the gastric digestion, 60 mL of gastric surimi was mixed with 60 mL of simulated intestinal fluid (SIF). The pH of the mixture was next regulated to 7.0 and shaken on a shaking table for 3 h (100 rpm, 37 °C). Samples were then collected for measurement at 0, 30, 60, 90, 120, 150, and 180 min.

2.6.4. Release rate and bioavailability of curcumin

The samples digested in simulated oral, gastric, and intestinal fluids at each time point were collected and centrifuged at 4000 rpm for 15 min, and the supernatant was taken to determine the curcumin content at 420 nm to calculate the curcumin release rate. In addition, after the intestinal digestion was completed, the digestive fluid was centrifuged (4000 rpm, 30 min), and the supernatant was taken to determine the curcumin content at 420 nm to calculate the bioavailability (Zou et al., 2016). The release rate and bioavailability of curcumin were calculated using Eq. (3) and Eq. (4) respectively:

$$Release\ rate\ (\%) = \frac{Release\ content\ of\ curcumin\ from\ supernatants}{Loading\ content\ of\ curcumin\ in\ nanocarriers} \times 100 \quad (3)$$

$$Bioavailability\ (\%) = \frac{Released\ curcumin\ after\ digestion\ completed}{Total\ curcumin\ before\ digestion} \times 100 \quad (4)$$

2.7. Statistical analysis

The results were expressed as mean ± standard deviation. Different groups were compared using one-way ANOVA and Waller-Duncan test at a significance level of 0.05 with the SPSS software (Version 25.0). There were three parallels in each group at least.

3. Results and discussion

3.1. Encapsulation efficiency (EE) and loading capacity (LC)

The EE and LC of TS-CUR, ASCP-TS-CUR, and ASP-TS-CUR were determined and shown in **Table 1**. Compared to TS-CUR, the EE of ASCP-TS-CUR and ASP-TS-CUR were significantly increased to 1.39-fold and 1.12-fold, respectively ($P < 0.05$). Likewise, the LC of ASCP-TS-CUR and ASP-TS-CUR were significantly increased to 1.37-fold and 1.11-fold, respectively ($P < 0.05$). The results indicated that the two modified nanocarriers effectively improved the encapsulation efficiency and loading capacity of curcumin. The reason may be that dioscin acted as a surfactant, reducing surface tension, decreasing the particle size of starch nanoparticles, and maintaining good dispersion of curcumin in starch granules, thus promoting the interaction between starch molecules and curcumin, which contributed to better encapsulating curcumin (Doost et al., 2018; Li et al., 2016a). Furthermore, the EE and LC of ASCP-TS-CUR were significantly higher than that of ASP-TS-CUR ($P < 0.05$). This difference may be attributed to that in the ASCP method, where curcumin, starch, and dioscin were

co-mixed, starch interacted with dioscin first, embedding a portion of dioscin into starch nanoparticles, which increased the contact between dioscin and curcumin, thereby enhancing the encapsulation effect of curcumin (Liu et al., 2022). In contrast, in the ASP method, dioscin was primarily encapsulated on the surface of the starch granules (Guo et al., 2020), resulting in a lower encapsulation efficiency. In previous studies, Zhong et al. (2024) prepared curcumin-loaded corn starch nanoparticles by self-assembly method and obtained similar EE (31.88 %–56.18 %) and LC (6.52 mg/g–7.99 mg/g). In addition, some studies coated curcumin with double-modified starch nanoparticles containing conjugated systems and obtained relatively higher LC (about 26 %) (Du et al., 2023; Wang et al., 2022). The discrepancy of LC in different systems may be attributed to differences in the amount of curcumin incorporated and the preparation method.

Table 1. EE and LC of TS-CUR, ASCP-TS-CUR, and ASP-TS-CUR.

Samples	EE (%)	LC (μg/mg)
TS-CUR	42.57 ± 1.21^{c}	5.24 ± 0.15^{c}
ASCP-TS-CUR	59.06 ± 1.73^{a}	7.18 ± 0.21^{a}
ASP-TS-CUR	47.68 ± 0.61^{b}	5.80 ± 0.07^{b}

Different lowercase letters in the same column indicate significant differences ($P < 0.05$).

3.2. Particle size and zeta potential

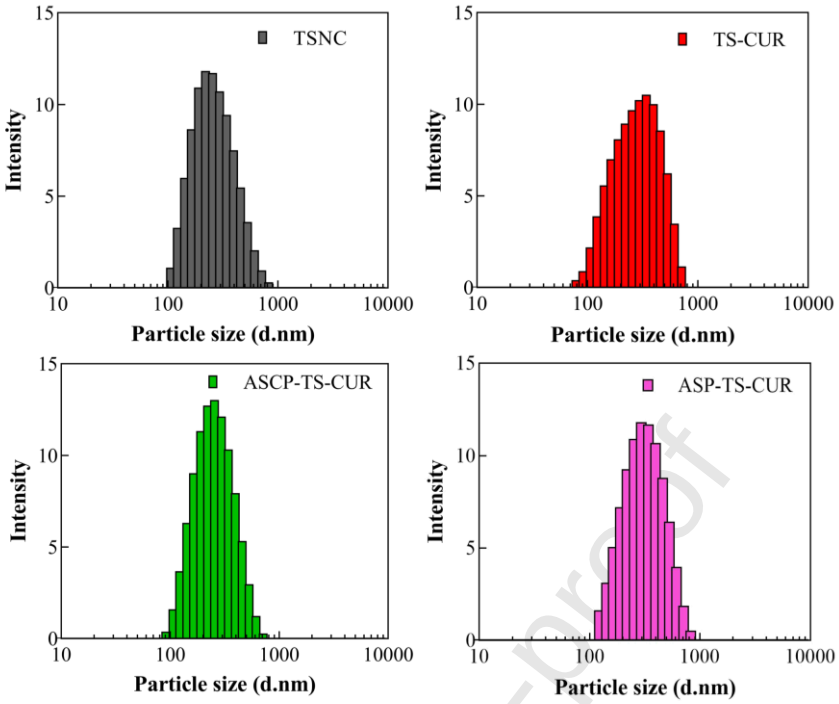

Fig. 2. Particle size distribution chart of TSNC, TS-CUR, ASCP-TS-CUR, and ASP-TS-CUR.

The particle size distribution chart of TSNC, TS-CUR, ASCP-TS-CUR, and ASP-TS-CUR was shown in **Fig. 2**, and their mean particle size, PDI, and zeta potential were recorded in **Table 2**. The mean particle size of TSNC was 227.10 ± 7.07 nm, and the increase in particle size after encapsulation may be due to the adsorption of curcumin onto the surface of starch nanoparticles (Remanan et al., 2024). This phenomenon was similar to the findings of Fu et al. (2018), who reported that the particle size of starch nanoparticles also increased after loading rutin. In addition, it was observed that the mean particle size and PDI of the two modified nanocarriers were significantly reduced compared to TS-CUR ($P < 0.05$), which emphasized the role of dioscin as a surfactant to control the particle size and improve the dispersion of the nanocarriers. This was demonstrated by the particle size distribution chart (**Fig. 2**). The

explanation given by Hu et al. (2015) is that during nucleation, the adsorption of surfactant molecules on the surface of the nucleus enables starch granules to avoid spatial repulsion for growth and therefore smaller starch nanoparticles can be formed. Moreover, ASCP-TS-CUR exhibited the smallest mean particle size (260.50 ± 9.01 nm). This may be attributed to the embedding of dioscin within the starch nanoparticles using the ASCP method, whereas in the ASP method, dioscin was encapsulated on the outside of the starch nanoparticles, resulting in a core-shell structure (Liu et al., 2022), and consequently, larger particle size for ASP-TS-CUR.

The zeta potential of TSNC was –10.93 ± 0.35 mV and the negative value was attributed to the ionization of hydroxyl groups in the nanoparticle surface (Sadeghi et al., 2017), while that of TS-CUR was significantly reduced to –12.83 ± 0.15 mV. The larger the absolute value of the zeta potential, the greater the stability of the system (Haseli et al., 2022). Notably, the absolute values of zeta potential of ASCP-TS-CUR and ASP-TS-CUR were lower than TS-CUR ($P < 0.05$). This reduction may be due to the binding of dioscin to the starch granules, resulting in a huge spatial site resistance between dioscin and the starch surface, thereby reducing the surface charge density of starch granules (Zembyla et al., 2020).

Table 2. The mean particle size, PDI, and zeta potential of TSNC, TS-CUR, ASCP-TS-CUR, and ASP-TS-CUR.

Samples	Mean particle size (nm)	PDI	Zeta potential (mV)
TSNC	227.10 ± 7.07^{c}	0.45 ± 0.07^{a}	$–10.93 \pm 0.35^{b}$

TS-CUR	325.23 ± 28.65[a]	0.44 ± 0.04[a]	–12.83 ± 0.15[c]
ASCP-TS-CUR	260.50 ± 9.01[b]	0.23 ± 0.03[c]	–10.23 ± 0.06[a]
ASP-TS-CUR	288.20 ± 7.62[b]	0.36 ± 0.02[b]	–10.10 ± 0.17[a]

Different lowercase letters in the same column indicate significant differences ($P < 0.05$).

3.3. FTIR analysis

The FTIR spectra of TSNC, TS-CUR, ASCP-TS-CUR, ASP-TS-CUR, and curcumin were shown in **Fig. 3A.** The FTIR spectra of TSNC were similar to that of TS (**Fig. S1A**). The absorption peak at 3300 cm^{-1} corresponded to the O–H stretching vibration of hydrogen bond (Sun et al., 2024). The band at 2923 cm^{-1} was linked to C–H stretching vibration, and the characteristic peak at 1640 cm^{-1} was associated with C=O vibration. Additionally, the band at 999 cm^{-1} was related to the C–O stretching vibration of the α-glucoside bond (Dankar et al., 2018). In the FTIR spectra of curcumin, absorption peaks appeared at 3500, 1625, 1601, 1502, 1428, 1272, and 1025 cm^{-1}, all of which were characteristic absorption peaks of curcumin (Li et al., 2016b; Mohan et al., 2012).

After loading curcumin, the FTIR spectra of TS-CUR, ASCP-TS-CUR, and ASP-TS-CUR were similar to that of TSNC; in other words, the characteristic peaks of curcumin almost disappeared. This suggested that the main spectral components of curcumin were weakened upon interaction with starch, indicating successful encapsulation into starch, which resulted in the masking of its FTIR absorption peaks (Jafari et al., 2016). Furthermore, the strength of the O–H absorption peaks (3300 cm^{-1}) in the composite nanocarriers was higher than in TSNC,

indicating that hydrogen bond interaction occurred between starch and curcumin molecules (Remanan et al., 2024). This finding was consistent with the results described by Baniani et al. (2019). Similarly, the peak strength at 1640 cm^{-1} (benzene ring tensile vibration of polyphenols) in the composite nanocarriers was increased, also indicating the presence of a hydrogen bond interaction between curcumin and the hydroxyl group of starch granules (Remanan et al., 2024). In addition, the increased absorption peak intensity at 999 cm^{-1} was attributed to the vibration of C−O−C in the glucose unit, which was thought to be a hydrogen bond interaction between curcumin and hydroxyl groups in different glucose units (Han et al., 2023). Ahmad et al. (2019) further demonstrated that hydrogen bonds play a dominant role in the interaction between starch molecules and phenolic substances.

Additionally, compared with TS-CUR, no new absorption peaks were observed in the FTIR spectra of ASCP-TS-CUR and ASP-TS-CUR, which indicated that the addition of dioscin did not alter the chemical structure of the nanocarriers (Huang et al., 2024). However, the absorption peak intensities of the modified nanocarriers at 3300 cm^{-1} and 999 cm^{-1} were further increased, suggesting that dioscin may enhance the hydrogen bonding interactions between starch and curcumin molecules.

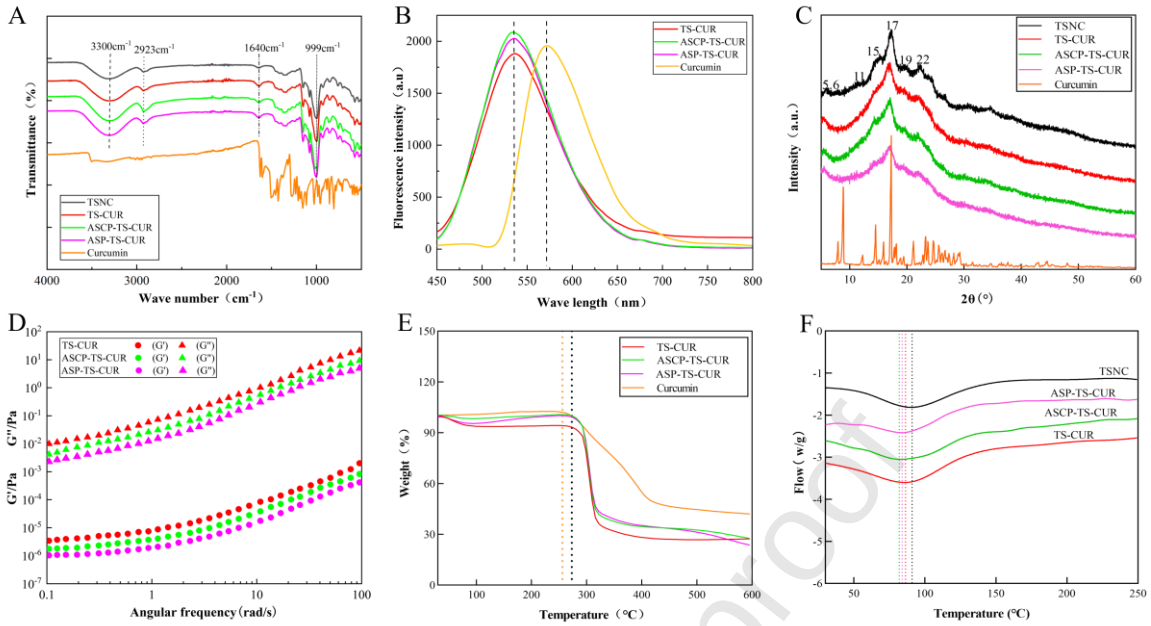

Fig. 3. The structural characteristics include FTIR spectra (A), fluorescence spectra (B), XRD patterns (C), dynamic rheogram (D), TG curves (E), and DSC patterns (F).

3.4. Fluorescence spectral analysis

The differences in molecular structure and electronic energy levels of different substances can lead to variations in peak shapes, positions, and intensities of fluorescence spectra. The fluorescence spectra of TS-CUR, ASCP-TS-CUR, and ASP-TS-CUR were determined and shown in **Fig. 3B**. The maximum absorption peak of free curcumin was observed at 571 nm, while the maximum absorption peak of curcumin in TS-CUR was blue shifted from 571 nm to 533 nm. This blue shift suggested that hydrogen bonding interactions between starch and curcumin molecules had occurred (Acevedo-Guevara et al., 2018), consistent with the previous study by Liang et al. (2023). A blue shift was reported in the maximum absorption spectrum of curcumin from 572 nm to 529 nm upon the formation of starch-curcumin nanoparticles,

confirming that the interaction between starch and curcumin was primarily hydrogen bonding (Liang et al., 2023). Notably, the fluorescence spectral peaks of ASCP-TS-CUR and ASP-TS-CUR were also blue-shifted to the same wavelengths as TS-CUR, but the peak intensity increased, especially for the ASCP method. This confirmed that a stronger interaction between curcumin, starch, and dioscin occurred in the ASCP method, which may be due to the stronger binding of dioscin to starch and curcumin during co-precipitation.

3.5. XRD analysis

The XRD patterns of TSNC, TS-CUR, ASCP-TS-CUR, ASP-TS-CUR, and curcumin were compared and shown in **Fig. 3C.** TSNC exhibited strong diffraction peaks near 2θ of 5.6°, 11°, 15°, 17°, 19°, and 22°. The peaks at 15° and 17° were characteristic of A-type crystalline starch, while the peaks at 5.6°, 17°, and 22° were typical peaks of B-type crystalline starch, suggesting that TSNC belongs to C-type crystal structure containing both A-type and B-type crystals (Cai et al., 2014; Guo et al., 2017). Previous studies have shown that a significant proportion of resistant starches and slow-digesting starches belong to C-type starch, which contributes to favorable glycemic responses and the proliferation of beneficial intestinal flora (Guo et al., 2017). Therefore, TSNC may also have great potential for applications in glycemic control and intestinal flora regulation.

The XRD pattern of curcumin was consistent with that reported by Han et al. (2023), exhibiting sharp and numerous diffraction peaks that indicate a highly crystalline structure. However, the characteristic peaks of curcumin disappeared in TS-CUR, ASCP-TS-CUR, and ASP-TS-CUR, and only broad starch diffraction peaks were observed at 2θ of 5.6°, 17°, 19°,

and 22°, indicating that curcumin was transformed into an amorphous form and existed inside the starch nanocarriers in an amorphous form (Choi et al., 2022). It has been reported that the amorphous structure has higher lattice-free energy, which contributes to improving the dissolution rate of water-insoluble substances, thus ensuring their good solubility and permeability in gastrointestinal digestive fluids, thereby facilitating their absorption and utilization (Ubeyitogullari et al., 2019). Therefore, encapsulation of curcumin in turmeric starch nanoparticles can improve its water solubility and availability. In addition, the peak at 2θ of 17° of ASCP-TS-CUR and ASP-TS-CUR was broadened with reduced intensity compared to TS-CUR, indicating a further decrease in crystallinity, which may be due to the addition of dioscin promoting the formation of hydrogen bonds between starch and curcumin, and further leading to the formation of more amorphous regions to encapsulate curcumin (Xiao et al., 2023). This is also confirmed by the improvement of encapsulation efficiency and loading capacity.

3.6. Rheological analysis

Dynamic rheology can be used to determine the viscoelastic properties of samples and has important applications in studying food processing characteristics and product quality control (Qiu et al., 2024). Two critical parameters in dynamic rheology are the energy storage modulus (G′) and the loss modulus (G″). G′ quantifies the energy stored during the elastic deformation of a material under applied stress, reflecting elasticity. G″ measures the energy dissipated during irreversible viscous deformation, indicating viscosity (Zhang et al., 2023). The effect of angular frequency on the dynamic modulus (G′ and G″) of TS-CUR, ASCP-TS-CUR, and ASP-TS-CUR mixture solutions was determined by dynamic rheology (**Fig. 3D)**. For all three

nanocarriers, G″ was larger than G′ across the entire frequency range, indicating that their viscous behavior was dominant over their elastic behavior. Furthermore, both G′ and G″ values increased gradually with the increase in angular frequency, showing an obvious frequency dependence. Moreover, the lower G′ and G″ values of ASCP-TS-CUR and ASP-TS-CUR compared with TS-CUR may be attributed to the modification of dioscin, which promoted the hydrogen bond interaction and encapsulation between starch molecules and curcumin, thus hindering the cross-linking between starch molecular chains, reducing the entanglement points of molecular chains in the starch gel system, further leading to the formation of a weaker starch gel network system, and accordingly reducing the dynamic moduli (G′ and G″) (Xiao et al., 2023). A similar phenomenon was reported by Zeng et al. (2022), whose results showed that the addition of polyphenols also reduced the G′ and G″ values of starch paste. This reduced dynamic modulus may have a positive effect on improving the texture and processing properties of starch-based carriers.

3.7. TG analysis

The TG curves of TS-CUR, ASCP-TS-CUR, ASP-TS-CUR, and curcumin were shown in **Fig. 3E**. Curcumin underwent only one stage of weight loss, starting from around 260 °C, whereas two stages of weight loss were observed in TS-CUR, ASCP-TS-CUR, and ASP-TS-CUR. The first stage occurred near 70 °C, attributed to the evaporation of water in starch samples, and the second stage occurred between 280 °C and 320 °C, due to the degradation of both starch and curcumin. In the second weight loss stage, the peak temperature of heat loss for free curcumin was approximately 270 °C, whereas those of nanocarriers

appeared around 300 °C, illustrating that the carrier materials effectively delayed the degradation temperature of curcumin and showed good thermal stability. A similar phenomenon was observed by Han et al. (2023), where porous starch nanoparticles effectively delayed the degradation temperature of curcumin. Furthermore, at the end of the second degradation phase, the final residual weight of ASCP-TS-CUR and ASP-TS-CUR was heavier than that of TS-CUR, suggesting that the modified nanocarriers had less weight loss and greater thermal stability. This may be related to the modification of dioscin, which may enhance the structural stability of the nanocarriers and retain more residual weight under high-temperature conditions, thus making it more advantageous in applications requiring high-temperature treatment.

3.8. DSC analysis

During starch gelatinization, starch granules absorbed water and swelled, leading to the melting of the crystalline layer of amylopectin and/or the disruption of the double helix structure formed by hydrogen bonding. This process was accompanied by an energetic change that was manifested as a heat-absorption peak on the DSC pattern, where the peak was the gelatinization temperature (Xing et al., 2017). **Fig. 3F** showed the DSC patterns of TSNC, TS-CUR, ASCP-TS-CUR, and ASP-TS-CUR. The heat absorption peak of TSNC appeared at 91 °C, while that of TS-CUR appeared at 86 °C after curcumin loading, which was related to the crystallinity. With lower crystallinity, the microcrystals can be disrupted and reorganized, thus lowering the heat required for gelatinization (Yan et al., 2024), which is manifested as a decrease in gelatinization temperature. Compared to TS-CUR, the heat absorption peaks of ASCP-TS-CUR and ASP-TS-CUR were reduced to 82 °C and 84 °C, respectively, further

lowering the gelatinization temperature. These results indicated that the modified nanocarriers had lower crystallinity and were more conducive to absorption and utilization, which was consistent with the results of XRD measurements.

3.9. Microstructure observation

The micromorphologic structures of TSNC, TS-CUR, ASCP-TS-CUR, and ASP-TS-CUR were observed by SEM, as presented in **Fig. 4**. Most of the TSNC showed an elliptical flattened lamellar structure with a flat and smooth surface and relatively uniform size, whereas the addition of curcumin altered the granular morphology of starch to more thread-like structures and increased the surface area, forming helix-like cavities. The increased surface area may improve the contact area with curcumin, potentially enhancing curcumin's activity. In addition, the aggregation of the two modified nanocarriers was more compact than TS-CUR, especially the ASCP-TS-CUR. This may be due to the incorporation of dioscin into starch nanoparticles in the ASCP method, resulting in a stronger interaction between dioscin, starch, and curcumin molecules, thus leading to a compact structure. This may reveal the reason for the smaller particle size of ASCP-TS-CUR. In addition, the TEM results (**Fig. 5**) further revealed that TSNC, TS-CUR, ASCP-TS-CUR, and ASP-TS-CUR were all nanometer scale, which was consistent with the particle size results in section 3.2.

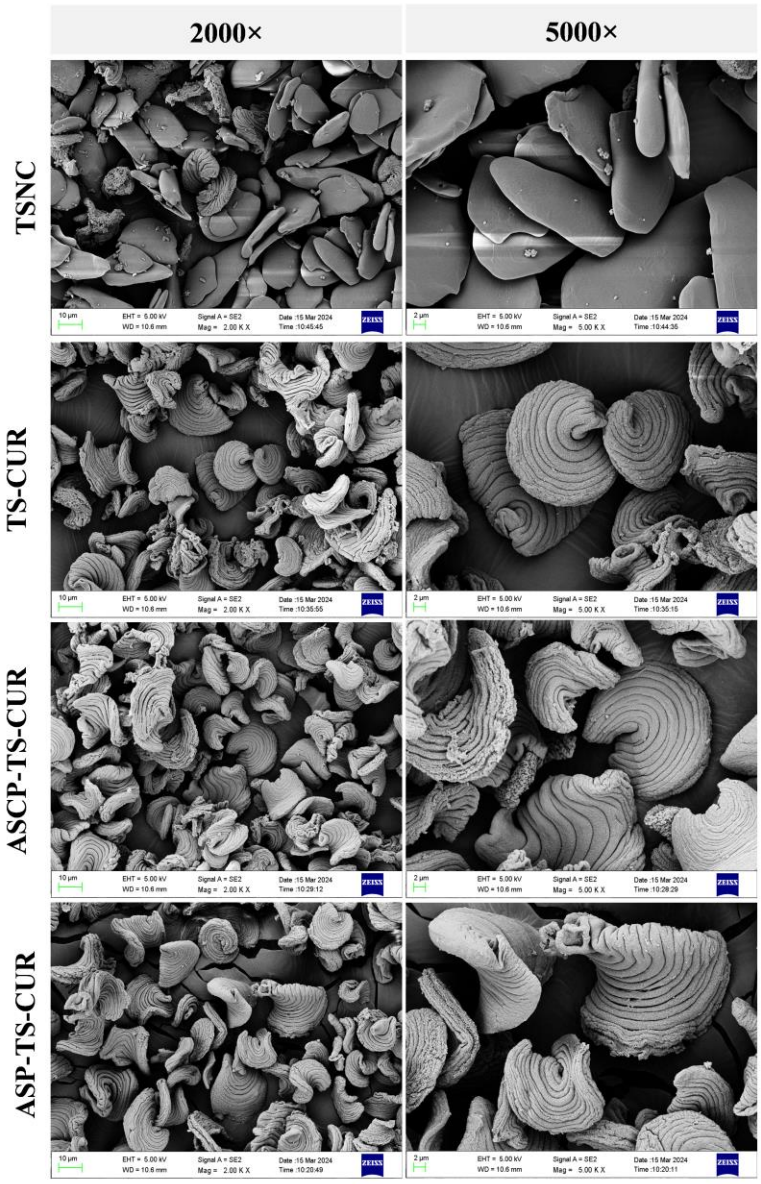

Fig. 4. SEM images of TSNC, TS-CUR, ASCP-TS-CUR, and ASP-TS-CUR (left, magnification 2000×; right, magnification 5000×).

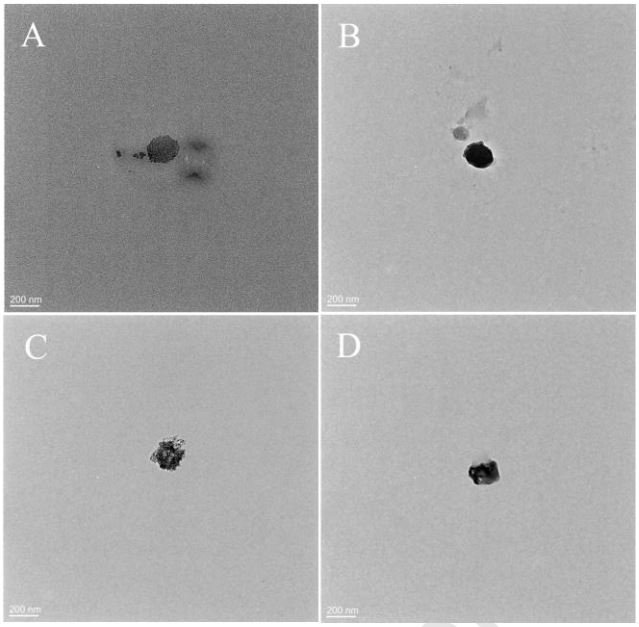

Fig. 5. TEM images of TSNC (A), TS-CUR (B), ASCP-TS-CUR (C), and ASP-TS-CUR (D).

3.10. Temperature stability

Heat treatment is widely applied in food processing, and the excellent thermal stability of nanocarriers can avoid the degradation of bioactive components, making temperature a key factor influencing the stability of nanocarriers (Zhu et al., 2023). **Fig. 6A, 6B, 6C, and 6D** showed the mean particle size, PDI, zeta potential, and curcumin retention rate of the three nanocarriers at different temperatures (30, 40, 50, 60, 70, 80, and 90 °C), respectively. As presented in **Fig. 6A**, the mean particle size of TS-CUR, ASCP-TS-CUR, and ASP-TS-CUR gradually decreased with increasing temperature, from 353.33 ± 4.58 nm, 247.23 ± 8.53 nm, and 267.47 ± 14.75 nm to the final 246.43 ± 11.15 nm, 182.13 ± 3.72 nm, and 189.63 ± 8.01 nm, respectively. This decrease was probably due to the increased solubility of starch with rising temperature, resulting in enhanced dispersion of starch granules, fewer large particles, and

reduced agglomeration. The PDI values of three nanocarriers were less than 0.5 (**Fig. 6B**), indicating a relatively uniform particle size distribution. Among them, ASCP-TS-CUR exhibited smaller variations in particle size and PDI across the whole temperature range, demonstrating better thermal stability.

The absolute values of zeta potential of TS-CUR, ASCP-TS-CUR, and ASP-TS-CUR gradually decreased from 16.43 ± 0.76 mV, 14.15 ± 0.49 mV, and 13.00 ± 0.57 mV to 11.97 ± 0.15 mV, 10.73 ± 0.71 mV, and 10.40 ± 0.28 mV (**Fig. 6C**), respectively. This decrease may be attributed to a reduction in the surface charge density of the nanocarriers caused by excessively high temperatures, leading to a decrease in the absolute value of the zeta potential (Gao et al., 2020).

The curcumin retention rate of the three nanocarriers showed a decreasing trend with the increase of temperature (**Fig. 6D**). At 90 °C, the curcumin retention rate of TS-CUR and ASP-TS-CUR was relatively low, which was 36.91 % and 41.27 % of their original level, respectively, whereas the curcumin retention rate of ASCP-TS-CUR was at 51.13%. The results indicated that the nanocarriers prepared by the ASCP method could better protect curcumin from degradation at high temperatures, which may be related to the stronger intermolecular interactions among dioscin, starch, and curcumin.

3.11. Ion stability

Composite nanocarriers will encounter a variety of complex ionic environments during the digestion and absorption process in the human gastrointestinal tract. The mean particle size, PDI, zeta potential, and curcumin retention rate of the three nanocarriers were determined at

different ionic concentrations (50, 100, 150, 200, and 250 mM), as shown in **Fig. 6E, 6F, 6G, and 6H**. As depicted in **Fig. 6E,** with increasing ion concentration, the mean particle size of TS-CUR showed an initial increase followed by a decrease. A maximum mean particle size of 696.10 ± 13.86 nm was observed at an ionic concentration of 100 mM, followed by a gradual decrease with increasing ion concentration. This increased effect may be due to the charge shielding effect generated by the salt ions reducing the repulsive force between nanoparticles, thereby inducing flocculation and agglomeration (An et al., 2021). However, excessively high ionic strength might lead to the dissociation of nanocarriers, resulting in a reduction in particle size (Chen et al., 2024). However, the mean particle size of ASCP-TS-CUR and ASP-TS-CUR only showed a gradually increasing trend throughout the whole range of ionic concentrations, increasing from 260.50 ± 9.01 nm and 288.20 ± 7.62 nm to 578.20 ± 14.99 nm and 614.55 ± 25.24 nm (**Fig. 6E**), respectively, indicating that ASCP-TS-CUR and ASP-TS-CUR effectively alleviated the influence of salt ions and avoided the dissociation of the carriers.

With the increase in ionic concentration, the PDI of TS-CUR, ASCP-TS-CUR, and ASP-TS-CUR all showed a gradually increasing trend (**Fig. 6F**), indicating a decrease in dispersion, whereas the ASCP method showed a relatively stable dispersity. The zeta potential results (**Fig. 6G**) showed that the three nanocarriers decreased significantly to around –2 to –4 mV after adding salt ions ($P < 0.05$). This decrease may be attributed to the enhanced adsorption of Na^+ on the nanocarriers, which produced electrostatic shielding or neutralization of the surface charge, thus weakening the electrostatic repulsion between the nanoparticles, finally resulting in a decrease in the absolute value of zeta potential (Liu et al., 2020).

The curcumin retention rate of the three nanocarriers gradually decreased with the increase of NaCl concentration (**Fig. 6H**). However, even at a salt ion concentration of 250 mM, the curcumin retention rate of TS-CUR and ASP-TS-CUR was above 90 %, and the retention rate of ASCP-TS-CUR was up to 95 %, which was still attributed to the stronger interaction in the ASCP method, thus providing a more powerful protective effect. In addition, Ai et al. (2023) reported that when curcumin was loaded into gum arabic nanoparticles, the retention rate of curcumin was about 85% at an ion concentration of 200 mM. These results indicated that the turmeric starch nanocarriers had good application potential in high-salt food systems.

3.12. pH stability

Nanocarriers will undergo significant pH changes within the gastrointestinal tract after being ingested, making it important to evaluate their pH stability for practical applications. The mean particle size, PDI, zeta potential, and curcumin retention rate of the three nanocarriers at different pH were shown in **Fig. 6I, 6G, 6K, and 6L** respectively. As shown in **Fig. 6I**, the nanocarriers were unstable under acidic conditions, with the mean particle size of TS-CUR, ASCP-TS-CUR, and ASP-TS-CUR all reaching maximum values at pH = 2 of 724.20 ± 12.18 nm, 515.35 ± 5.44 nm, and 533.10 ± 11.50 nm, respectively. Subsequently, with an increase in pH, the mean particle size of TS-CUR, ASCP-TS-CUR, and ASP-TS-CUR gradually decreased to 557.97 ± 2.85 nm, 206.05 ± 6.92 nm, and 234.15 ± 0.64 nm, respectively. The trend of PDI (**Fig. 6G**) was similar to that of mean particle size, indicating that the stability of nanocarriers gradually recovered as the environment changed from acidic to neutral conditions. In addition, the mean particle size of ASCP-TS-CUR and ASP-TS-CUR were smaller than TS-CUR, with

significant differences ($P < 0.05$), suggesting that the effect of pH on the particle size of modified nanocarriers was much smaller.

The zeta potential results showed that the absolute zeta potential value of TS-CUR, ASCP-TS-CUR, and ASP-TS-CUR was small at low pH, approximately 2 to 3 mV (**Fig. 6K**), likely due to the decrease in the surface charge of the granules in an acidic environment, leading to decreased system stability. However, with the increase of pH, the absolute value of the zeta potential of TS-CUR, ASCP-TS-CUR, and ASP-TS-CUR gradually increased to 12.47 ± 0.25 mV, 14.01 ± 0.41 mV, and 13.40 ± 0.29 mV, respectively, and the aggregation phenomenon was also improved, suggesting that the nanocarriers were more stable in a neutral environment.

In addition, the curcumin retention rate of the three nanocarriers generally increased first and then stabilized with the increase of pH (**Fig. 6L**). It can be expected that the curcumin retention rate of TS-CUR, ASCP-TS-CUR, and ASP-TS-CUR was the lowest when pH = 2, but still could reach 87.01 %, 95.92 %, and 92.08 %, respectively, and the higher and stable retention rate occurred at pH = 6–8. In contrast, Zhong et al. (2024) reported that the curcumin retention rate in debranched corn starch nanoparticles was only 71 % at pH = 9. These results indicated that our nanocarriers had good pH stability in a neutral environment. Moreover, the retention rate of curcumin in ASCP-TS-CUR was higher than the other two nanocarriers. This improvement can be attributed to the stronger hydrogen bond interaction between dioscin, starch, and curcumin in the ASCP method, which can provide a stronger physical barrier for curcumin (Zhong et al., 2024).

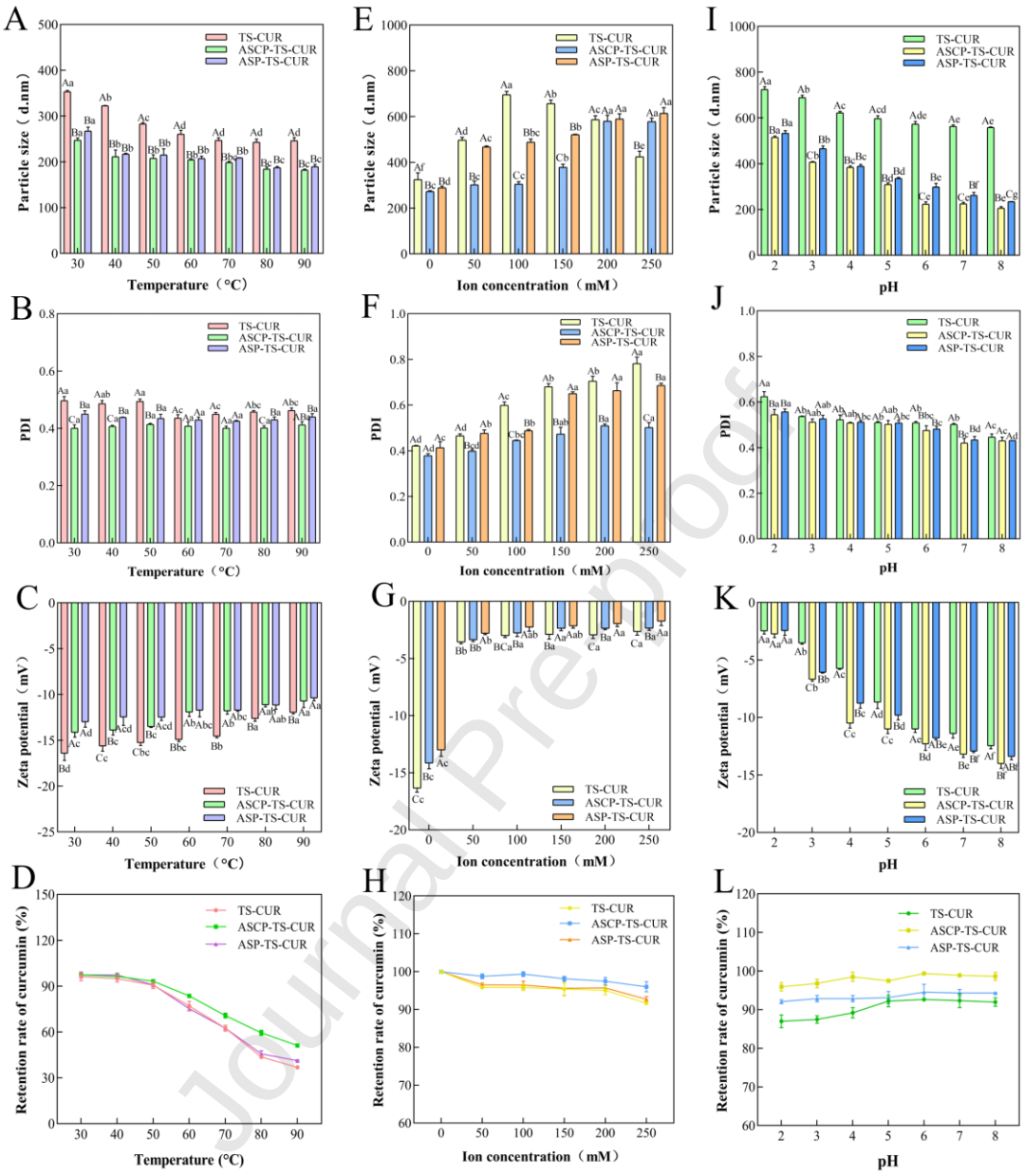

Fig. 6. The mean particle size (A), PDI (B), zeta potential (C), and curcumin retention rate (D) of TS-CUR, ASCP-TS-CUR, and ASP-TS-CUR at different temperatures; the mean particle size (E), PDI (F), zeta potential (G), and curcumin retention rate (H) of TS-CUR, ASCP-TS-CUR, and ASP-TS-CUR at different ion concentrations; the mean particle size (I), PDI (G), zeta potential (K), and curcumin retention rate (L) of TS-CUR, ASCP-TS-CUR, and

ASP-TS-CUR at different pH.

Different lowercase letters indicate significant differences in a sample at different temperatures, ion concentrations, or pH ($P < 0.05$), and different capital letters indicate significant differences between different samples at the same temperature, ion concentrations, or pH ($P < 0.05$).

3.13. Storage stability

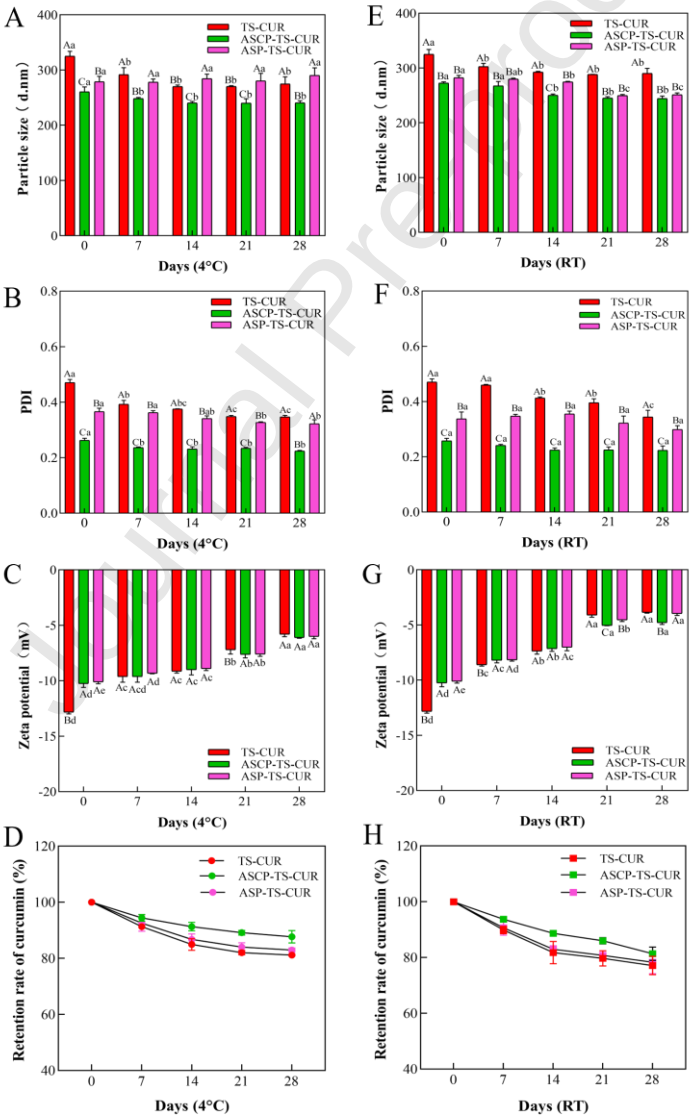

Fig. 7. The mean particle size (A), PDI (B), zeta potential (C), and curcumin retention rate (D)

of TS-CUR, ASCP-TS-CUR, and ASP-TS-CUR at 4 °C; the mean particle size (E), PDI (F), zeta potential (G), and curcumin retention rate (H) of TS-CUR, ASCP-TS-CUR, and ASP-TS-CUR at RT.

Different lowercase letters indicate significant differences between a sample on different days ($P < 0.05$); different capital letters indicate significant differences between different samples on the same days ($P < 0.05$).

Storage stability is an important index for assessing the stability of the complex and indicating its potential shelf life in commercial applications. The variations in mean particle size, PDI, zeta potential, and curcumin retention rate at 4 °C and RT for TS-CUR, ASCP-TS-CUR, and ASP-TS-CUR were presented in **Fig. 7**. Under both storage conditions, the mean particle size (280–320 nm) and PDI (0.4–0.5) of TS-CUR fluctuated with the increase in storage time. However, the mean particle size of ASCP-TS-CUR and ASP-TS-CUR only fluctuated slightly, remaining around 250–260 nm and 280–290 nm respectively (**Fig. 7A, 7E**), and the PDI also changed little (**Fig. 7B, 7F**), indicating that the modified nanocarriers had better stability throughout the 28-day storage period. The absolute value of the zeta potential of TS-CUR, ASCP-TS-CUR, and ASP-TS-CUR exhibited a gradual decrease with the increasing storage time (**Fig. 7C, 7G**), possibly due to the electrostatic repulsion of the carriers being affected over time. The curcumin retention rate of nanocarriers was further determined under 4 °C and RT. The results showed that the curcumin retention rate of TS-CUR, ASCP-TS-CUR, and ASP-TS-CUR was above 80 % after 28-day storage (**Fig. 7D, 7H**). Similar results were reported by Chen et al. (2024), when curcumin was encapsulated in octenyl succinic

anhydride-modified starch nanoparticles and stored for one month, the degradation of curcumin was about 20 %. Moreover, the retention rate of two modified nanocarriers was higher than TS-CUR, possibly due to the antioxidant properties of dioscin, which inhibited the degradation of curcumin. In particular, the highest retention rate in ASCP-TS-CUR implied that the ASCP method was more effective in preserving curcumin, which may be attributed to its smaller particle size and more stable performance (Liu et al., 2022).

3.14. In vitro release and bioavailability of curcumin in nanocarriers

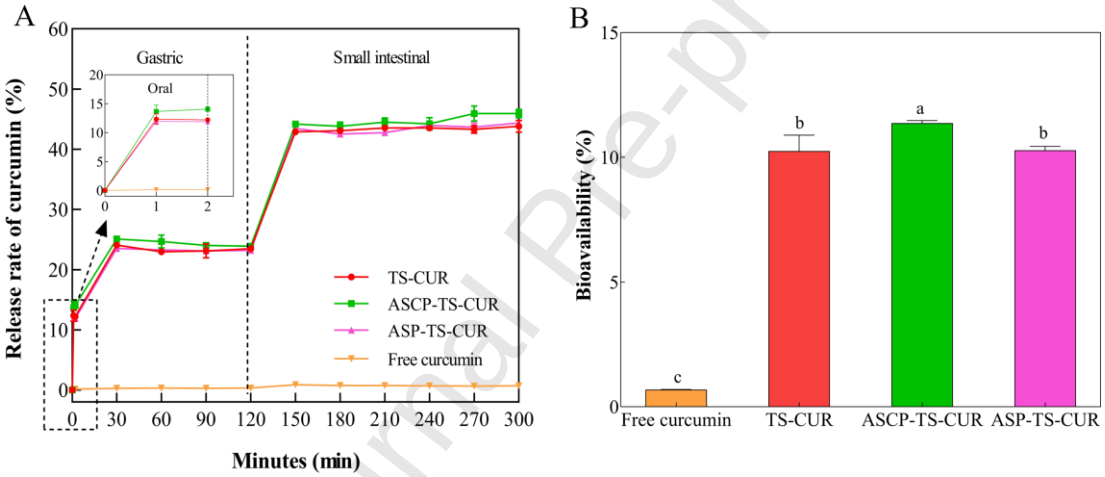

Fig. 8. *In vitro* release rate (A) and bioavailability (B) of curcumin in free curcumin, TS-CUR, ASCP-TS-CUR, and ASP-TS-CUR.

Different lowercase letters indicate significant differences ($P < 0.05$).

The *in vitro* release properties and bioavailability of curcumin were determined and shown in **Fig. 8**. Unsurprisingly, due to the poor water solubility of curcumin, the cumulative release rate (< 2 %) and bioavailability (~ 0.6%) of free curcumin was very low throughout the simulated release period. In contrast, TS-CUR, ASCP-TS-CUR, and ASP-TS-CUR showed a

similar persistent release trend throughout the simulated digestion phase (**Fig. 8A**). At the end of the oral digestion phase (2 min), the release rate of curcumin in TS-CUR, ASCP-TS-CUR, and ASP-TS-CUR reached 12.11 %, 14.38 %, and 11.88 %, respectively. This may be attributed to the action of amylase during the oral phase. At the end of gastric digestion (120 min), the curcumin release rate of TS-CUR, ASCP-TS-CUR, and ASP-TS-CUR reached 23.46 %, 24.24 %, and 23.20 %, respectively. This increase was attributed to the strong acidic environment of gastric juice which weakened the interaction between curcumin and starch, allowing more curcumin to be released (Xu et al., 2024). However, the release rate was stable during the gastric digestion stage, indicating that starch nanocarriers still had a protective effect on curcumin. Subsequently, during the small intestinal digestion stage, the curcumin release rate of TS-CUR, ASCP-TS-CUR, and ASP-TS-CUR were significantly increased to 43.82 %, 45.96 %, and 44.36 %, respectively, which were about 22–23 time higher than that of free curcumin. This may be due to the changes in pH and ionic strength as the environment shifted from acidic to neutral, which triggered a sudden release of curcumin in the intestine. Li et al. (2016b) also reported a similar sudden release of curcumin loaded in corn starch nanoparticles in SGF and SIF. This targeted intestinal release profile facilitated curcumin's bioactivity in the intestine. Additionally, the release curve showed a persistent release, indicating its potential suitability for long-term drug delivery (Zhang et al., 2025). **Fig. 8B** further showed that the bioavailability of curcumin in the three nanocarriers was approximately 17–20 times higher than free curcumin ($P < 0.05$). These results suggested that TS-CUR, ASCP-TS-CUR, and ASP-TS-CUR significantly improve the intestinal targeted release of curcumin, especially the

ASCP-TS-CUR, which might be related to the smaller particle size and better stability of the ASCP method.

4. Conclusion

In this study, two modified turmeric starch nanocarriers were successfully synthesized by ASCP and ASP methods using dioscin as a natural surfactant, and curcumin was effectively encapsulated and protected. FTIR results revealed that curcumin was successfully encapsulated in turmeric starch nanocarriers, and ASCP-TS-CUR and ASP-TS-CUR exhibited similar functional groups to TS-CUR, but the two modified nanocarriers had enhanced hydrogen bond interactions. TGA, DSC, and physical stability evaluation showed that ASCP-TS-CUR had better physical stability and storage stability. Furthermore, both ASCP and ASP methods effectively improved the encapsulation performance of starch nanocarriers, especially the ASCP method produced smaller particle size, higher encapsulation efficiency, and better loading capacity. Additionally, *in vitro* digestion studies showed that the release rate and bioavailability of ASCP-TS-CUR were approximately 23 and 20 times higher than free curcumin, respectively. Overall, the natural surfactant, dioscin, was successfully used to reduce the particle size of starch nanocarriers and improve the encapsulation properties, especially the ASCP method was proved to offer a better modification effect. These findings provide a new strategy for designing green and high-performance nanocarriers to deliver and protect hydrophobic components, which will be beneficial for promoting innovation and development in the field of drug delivery.

CRediT authorship contribution statement

Wenqing Zhu: Writing-original draft, Methodology, Investigation, Formal analysis, Data curation, Conceptualization. **Xinyan Bai**: Visualization, Data curation. **Wenbo Du**: Resources, Investigation. **Lingyu Li**: Writing-review and editing, Data curation. **Marie-Laure Fauconnier, & Aurore Richel**: Writing-review and editing, Supervision. **Hongjing Dong:** Writing-review and editing. **Zhenjia Zheng**: Writing-review and editing, Supervision, Resources, Project administration, Funding acquisition, Conceptualization.

Acknowledgments

This work was supported by the Key Research and Development Program of Shandong Province, China (2021CXGC010508) and the Innovation Capacity Enhancement Project of Medium and Small Enterprises of Science and Technology in Shandong Province, China (2024TSGC0483).

References

Araiza-Calahorra, A., & Sarkar, A. (2019). Pickering emulsion stabilized by protein nanogel particles for delivery of curcumin: Effects of pH and ionic strength on curcumin retention. *Food Structure, 21,* 100113. https://doi.org/10.1016/j.foostr.2019.100113

Acevedo-Guevara, L., Nieto-Suaza, L., Sanchez, L. T., Pinzon, M. I., & Villa, C. C. (2018). Development of native and modified banana starch nanoparticles as vehicles for curcumin. *International Journal of Biological Macromolecules, 111*, 498–504. https://doi.org/10.1016/j.ijbiomac.2018.01.063

Argel-Pérez, S., Gañán-Rojo, P., Cuartas-Marulanda, D., Gómez-Hoyos, C., Velázquez-Cock, J.,

Vélez-Acosta, L., Zuluaga, R., & Serpa-Guerra, A. (2023). Characterization of a novel starch isolated from the rhizome of Colombian turmeric (*Curcuma longa* L.) cultivars. *Foods*, *13*(1), 7. https://doi.org/10.3390/foods13010007

Ahmad, M., Mudgil, P., Gani, A., Hamed, F., Masoodi, F. A., & Maqsood, S. (2019). Nano-encapsulation of catechin in starch nanoparticles: Characterization, release behavior and bioactivity retention during simulated *in-vitro* digestion. *Food Chemistry, 270*, 95-104. https://doi.org/10.1016/j.foodchem.2018.07.024

An, S. Y., Wang, L., Zhou, P., Luo, Z., Feng, R., & Li, X. Y. (2021). Construction of *Hohenbuehelia serotina* polysaccharides-mucin nanoparticles and their sustain-release characteristics under simulated gastrointestinal digestion *in vitro*. *International Journal of Biological Macromolecules*, *191*, 1–8. https://doi.org/10.1016/j.ijbiomac.2021.09.068

Ai, C., Zhao, C. G., Xiang, C. H., Zheng, Y. M., Zhong, S. Y., Teng, H., & Chen, L. (2023). Gum arabic as a sole wall material for constructing nanoparticle to enhance the stability and bioavailability of curcumin. *Food Chemistry: X*, *18*, 100724. https://doi.org/10.1016/j.fochx.2023.100724

Bandopadhyay, S., Anand, U., Gadekar, V. S., Jha, N. K., Gupta, P. K., Behl, T., Kumar, M., Radha, Shekhawat, M. S., & Dey, A. (2022). Dioscin: A review on pharmacological properties and therapeutic values. *Biofactors*, *48*(1), 22–25. https://doi.org/10.1002/biof.1815

Blanco, E., Shen, H., & Ferrari, M. (2015). Principles of nanoparticle design for overcoming biological barriers to drug delivery. *Nature Biotechnology, 33*(9), 941–951.

https://doi.org/10.1038/nbt.3330

Baniani, D. D., Zahedifar, P., Bagheri, R., & Solouk, A. (2019). Curcumin-loaded starch micro/nano particles for biomedical application: the effects of preparation parameters on release profile. *Starch-Starke, 71*, 1800305. https://doi.org/10.1002/star.201800305

Bu, X. T., Guan, M. H., Dai, L., Ji, N., Qin, Y., Xu, X. F., Xiong, L., Shi, R., & Sun, Q. J. (2023). Fabrication of starch-based emulsion gel beads by an inverse gelation technique for loading proanthocyanidin and curcumin. *Food Hydrocolloids*, *137*, 108336. https://doi.org/10.1016/j.foodhyd.2022.108336

Chen, Y. Y., Liu, K., Zha, X. Q., Li, Q. M., Pan, L. H., & Luo, J. P. (2021). Encapsulation of luteolin using oxidized lotus root starch nanoparticles prepared by anti-solvent precipitation. *Carbohydrate Polymers*, *273*, 118552. https://doi.org/10.1016/j.carbpol.2021.118552

Chen, X. L., Li, L. Y., Zhu, W. Q., Teng, Y., Qiu, Z. C., Ji, W. H., Zheng, Z. J., & Gong, J. Q. (2024). Fabrication of caffeoylquinic acid-loaded burdock polysaccharide nanoparticles and their antioxidant activity in hydrogen peroxide-damaged HepaRG cells. *Food Chemistry: X*, *22*, 101293. https://doi.org/10.1016/j.fochx.2024.101293

Chen, C. Y., Wang, Z. X., Fu, H. L., Yu, G. Q., Luo, X., & Zhu, K. W. (2024). Enhanced bioavailability of curcumin amorphous nanocomposite prepared by a green process using modified starch. *International Journal of Biological Macromolecules*, *270*, 132210. https://doi.org/10.1016/j.ijbiomac.2024.132210

Choi, I., Li, N., & Zhong, Q. X. (2022). Enhancing bioaccessibility of resveratrol by loading in

natural porous starch microparticles. *International Journal of Biological Macromolecules, 194*, 982–992. https://doi.org/10.1016/j.ijbiomac.2021.11.157

Cai, J. W., Cai, C. H., Man, J. M., Zhou, W. D., & Wei, C. X. (2014). Structural and functional properties of C-type starches. *Carbohydrate Polymers, 101*, 289-300. https://doi.org/10.1016/j.carbpol.2013.09.058

Du, Y. J., Chu, J. M., Wang, R. X., Zhang, C. L., Zhang, J., & Zhi, K. K. (2023). Efficient encapsulation of fat-soluble food-derived biofunctional substances (curcumin as an example) in dual-modified starch-based nanoparticles containing large conjugated systems. *International Journal of Biological Macromolecules, 242*, 125078. https://doi.org/10.1016/j.ijbiomac.2023.125078

Doost, A. S., Camp, J. V., Dewettinck, K., & Meeren, P. V. D. (2019). Production of thymol nanoemulsions stabilized using Quillaja Saponin as a biosurfactant: Antioxidant activity enhancement. *Food Chemistry, 293*, 134–143. https://doi.org/10.1016/j.foodchem.2019.04.090

Dankar, I., Haddarah, A., Omar, F. E. L., Pujolà, M., & Sepulcre, F. (2018). Characterization of food additive-potato starch complexes by FTIR and X-ray diffraction. *Food Chemistry, 260*, 7–12. https://doi.org/10.1016/j.foodchem.2018.03.138

Doost, A. S., Muhammad, D. R. A., Stevens, C. V., Dewettinck, K., & Meeren, P. V. (2018). Fabrication and characterization of quercetin loaded almond gum-shellac nanoparticles prepared by antisolvent precipitation. *Food Hydrocolloids, 83*, 190–201. https://doi.org/10.1016/j.foodhyd.2018.04.050

Ferguson, J. J. A., Abbott, K. A., Garg, M. L. (2021). Anti-inflammatory effects of oral supplementation with curcumin: a systematic review and meta-analysis of randomized controlled trials. *Nutrition Reviews, 79*, 1043–1066. https://doi.org/10.1093/nutrit/nuaa114

Fu, Y. J., Yang, J. D., Jiang, L. W., Ren, L. L., & Zhou, J. (2018). Encapsulation of lutein into starch nanoparticles to improve its dispersity in water and enhance stability of chemical oxidation. *Starch-Strke, 71(19)*, 19-25. https://doi.org/10.1002/star.201800248

Guo, Z. B., Zeng, S. Y., Lu, X., Zhou, M. L., Zheng, M. J., & Zheng, B. D. (2015). Structural and physicochemical properties of lotus seed starch treated with ultra-high pressure. *Food Chemistry, 186*, 223–230. https://doi.org/10.1016/j.foodchem.2015.03.069

Guo, Q., Su, J. Q., Shu, X., Yuan, F., Mao, L. K., & Gao, Y. X. (2020). Development of high methoxyl pectin-surfactant-pea protein isolate ternary complexes: Fabrication, characterization and delivery of resveratrol. *Food Chemistry, 321*, 126706. https://doi.org/10.1016/j.foodchem.2020.126706

Guo, Z. B., Jia, X. Z., Zhao, B. B., Zeng, S. X., Xiao, J. B., & Zheng, B. D. (2017). C-type starches and their derivatives: structure and function. *Annals of the New York Academy of Sciences, 1398*(1), 47–61. https://doi.org/10.1111/nyas.13351

Gao, X., Li, X. F., Mu, J. J., Ho, C. T., Su, J. Y., Zhang, Y. T., Lin, X. R., Chen, Z. Z., Li, B., & Xie, Y. Z. (2020). Preparation, physichemical characterization, and anti-proliferation of selenium nanoparticles stabilized by polyporus umbellatus polysaccharide. *International Journal of Biological Macromolecules, 152*, 605–615. https://doi.org/10.1016/j.ijbiomac.2020.02.199

Henao-Ardila, A., Quintanilla-Carvajal, M. X., & Moreno, F. L. (2024). Emulsification and stabilisation technologies used for the inclusion of lipophilic functional ingredients in food systems. *Heliyon, 10*, e32150. https://doi.org/10.1016/j.heliyon.2024.e32150

Han, X. Y., Ma, P., Shen, M. Y., Wen, H. L., & Xie, J. H. (2023). Modified porous starches loading curcumin and improving the free radical scavenging ability and release properties of curcumin. *Food Research International, 168*, 112770. https://doi.org/10.1016/j.foodres.2023.112770

Hu, K., & McClements, D. J. (2015). Fabrication of biopolymer nanoparticles by antisolvent precipitation and electrostatic deposition: Zein-alginate core/shell nanoparticles. *Food Hydrocolloids, 44*, 101–108. https://doi.org/10.1016/j.foodhyd.2014.09.015

Huang, S. Y., Zhu, X. N., Ma, S., Kim, Y. R., & Luo, K. (2024). Tween 80-mediated size-controlled self-assembly of resistant starch particle: A green and biodegradable white pigment for food applications. *Food Hydrocolloids, 153*, 109993. https://doi.org/10.1016/j.foodhyd.2024.109993

Haseli, S., Pourmadadi, M., Samadi, A., Yazdian, F., Abdouss, M., Rashedi, H., & Navaei-Nigjeh, M. (2022). A novel pH-responsive nanoniosomal emulsion for sustained release of curcumin from a chitosan-based nanocarrier: Emphasis on the concurrent improvement of loading, sustained release, and apoptosis induction. *Biotechnology Progress, 38*, e3280. https://doi.org/10.1002/btpr.3280

Jafari, Y., Sabahi, H., & Rahaie, M. (2016). Stability and loading properties of curcumin encapsulated in Chlorella vulgaris. *Food Chemistry, 211*, 700–706.

https://doi.org/10.1016/j.foodchem.2016.05.115

Karaca, A. C., Rezaei, A., Qamar, M., Assadpour, E., Esatbeyoglu, T., & Jafari, S. M. (2025). Lipid-based nanodelivery systems of curcumin: Recent advances, approaches, and applications. *Food Chemistry, 463*, 141193. https://doi.org/10.1016/j.foodchem.2024.141193

Kuttigounder, D., Lingamallu, J. R., & Bhattacharya, S. (2011). Turmeric powder and starch: selected physical, physicochemical, and microstructural properties. *Journal of Food Science, 76*(9), C1284–C1291. https://doi.org/10.1111/j.1750-3841.2011.02403.x

Li, X. J., Qin, Y., Liu, C. Z., Jiang, S. S., Xiong, L., & Sun, Q. J. (2016a). Size-controlled starch nanoparticles prepared by self-assembly with different green surfactant: The effect of electrostatic repulsion or steric hindrance. *Food Chemistry, 199*, 356–363. https://doi.org/10.1016/j.foodchem.2015.12.037

Li, J. L., Shin, G. H, Lee, I. W., Chen, X. G., & Park, H. L. (2016b). Soluble starch formulated nanocomposite increases water solubility and stability of curcumin. *Food Hydrocolloids, 56*, 41–49. https://doi.org/10.1016/j.foodhyd.2015.11.024

Liao, Y. Y., Li, Z. X., Zhou, Q., Sheng, M. K., Qu, Q. S., Shi, Y. S., Yang, J. Q., Lv, L. J., Dai, X. X., & Shi, X. Y. (2021). Saponin surfactants used in drug delivery systems: A new application for natural medicine components. *International Journal of Pharmaceutics, 603*, 120709. https://doi.org/10.1016/j.ijpharm.2021.120709

Liu, C. R., Xu, B. X., McClements, D. J., Xu, X. Y., Cui, S., Gao, L., Zhou, L. Y., Xiong, L., Sun, Q. J., & Dai, L. (2022). Properties of curcumin-loaded zein-tea saponin nanoparticles

prepared by antisolvent co-precipitation and precipitation. *Food Chemistry, 391*, 133224. https://doi.org/10.1016/j.foodchem.2022.133224

Liu, Q. G., Han, C. P., Tian, Y. M., & Liu, T. Y. (2020). Fabrication of curcumin-loaded zein nanoparticles stabilized by sodium caseinate/sodium alginate: Curcumin solubility, thermal properties, rheology, and stability. *Process Biochemistry, 94*, 30–38. https://doi.org/10.1016/j.procbio.2020.03.017

Liu, Q., Li, F., Ji, N., Dai, L., Xiong, L., & Sun, Q. J. (2021). Acetylated debranched starch micelles as a promising nanocarrier for curcumin. *Food Hydrocolloids, 111*, 106253. https://doi.org/10.1016/j.foodhyd.2020.106253

Marefati, A., Bertrand, M., Sjöö, M., Dejmek, P., & Rayner, M. (2017). Storage and digestion stability of encapsulated curcumin in emulsions based on starch granule Pickering stabilization. *Food Hydrocolloids, 63,* 309–320. https://doi.org/10.1016/j.foodhyd.2016.08.043

Mohan, P. R. K., Sreelakshmi, G., Muraleedharan, C. V., & Joseph, R. (2012). Water soluble complexes of curcumin with cyclodextrins: Characterization by FT-Raman spectroscopy. *Vibrational Spectroscopy, 62*, 77–84. https://doi.org/10.1016/j.vibspec.2012.05.002

Qiu, Z. C., Li, L. Y., Zhu, W. Q., Qiao, X. G., Zheng, Z. J., & Sun-Waterhouse, D. X. (2024). Pectins rich in RG-I and galactose extracted from garlic pomace: Physicochemical, structural, emulsifying and antioxidant properties. *Food Hydrocolloids, 149*, 109559. https://doi.org/10.1016/j.foodhyd.2023.109559

Rasmi, Y., Kırboğa, K. K., Tekin, B., & Demir, M. (2024). Chapter 13 - Turmeric starch:

structure, functionality, and applications. In J. M. Lorenzo, & S. P. Bangar (Eds.), *Non-Conventional Starch Sources* (pp. 377–405). Academic Press. https://doi.org/10.1016/B978-0-443-18981-4.00013-6

Remanan, M. K., & Zhu, F. (2024). Encapsulation of chrysin and rutin using self-assembled nanoparticles of debranched quinoa, maize, and waxy maize starches. *Carbohydrate Polymers*, *337*, 122118. https://doi.org/10.1016/j.carbpol.2024.122118

Sadeghi, R., Daniella, Z., Uzun, S., & Kokini, J. (2017). Effects of starch composition and type of non-solvent on the formation of starch nanoparticles and improvement of curcumin stability in aqueous media. *Journal of Cereal Science*, *76*, 122–130. https://doi.org/10.1016/j.jcs.2017.05.020

Sun, C. X., Dai, L., & Gao, Y. X. (2016). Binary complex based on zein and propylene glycol alginate for delivery of Quercetagetin. *Biomacromolecules*, *17*, 3973–3985. https://doi.org/10.1021/acs.biomac.6b01362

Sun, Q. J., Li, G. H., Dai, L., Ji, N., & Xiong, J. L. (2024). Green preparation and characterisation of waxy maize starch nanoparticles through enzymolysis and recrystallisation. *Food Chemistry*, *162*, 223–228. https://doi.org/10.1016/j.foodchem.2014.04.068

Song, X. X., Chen, Y. Y., Sun, H. B., Liu, X. N., & Leng, X. J. (2021). Physicochemical stability and functional properties of selenium nanoparticles stabilized by chitosan, carrageenan, and gum Arabic. *Carbohydrate Polymers*, *255*, 117379. https://doi.org/10.1016/j.carbpol.2020.117379

Tao, X. F., Yin, L. H., Xu, L. N., & Peng, J. Y. (2018). Dioscin: A diverse acting natural compound with therapeutic potential in metabolic diseases, cancer, inflammation and infections. *Pharmacological Research, 137*, 259–269. https://doi.org/10.1016/j.phrs.2018.09.022

Ubeyitogullari, A., & Ciftci, O. N. (2019). A novel and green nanoparticle formation approach to forming low-crystallinity curcumin nanoparticles to improve curcumin's bioaccessibility. *Scientific Reports, 9*, 19112. https://doi.org/10.1038/s41598-019-55619-4

Wang, Y. L., Ou, X. Q., Maqtari, Q. A. A., He, H. J., & Othman, N. (2024). Evaluation of amylose content: Structural and functional properties, analytical techniques, and future prospects. *Food Chemistry: X, 24*, 101830. https://doi.org/10.1016/j.fochx.2024.101830

Wang, X. J., Li, M., Liu, F. G., Peng, F., Li, F., Lou, X. M., Jin, Y., Wang, J., & Xu, H. D. (2021). Fabrication and characterization of zein-tea polyphenols-pectin ternary complex nanoparticles as an effective hyperoside delivery system: Formation mechanism, physicochemical stability, and *in vitro* release property. *Food Chemistry, 364*, 130335. https://doi.org/10.1016/j.foodchem.2021.130335

Wang, R. X., Qin, X. Y., Du, Y. J., Shan, Z. G., Shi, C., Huang, K. R., Wang, J. C., & Zhi, K. K. (2022). Dual-modified starch nanoparticles containing aromatic systems with highly efficient encapsulation of curcumin and their antibacterial applications. *Food Research International, 162*, 111926. https://doi.org/10.1016/j.foodres.2022.111926

Xiang, C. Y., Gao, J., Ye, H. X., Ren, G. R., Ma, X. J., Xie, H. J., Fang, S., Lei, Q. F., & Fang, W. J. (2020). Development of ovalbumin-pectin nanocomplexes for vitamin D_3

encapsulation: Enhanced storage stability and sustained release in simulated gastrointestinal digestion. *Food Hydrocolloids, 106*, 105926. https://doi.org/10.1016/j.foodhyd.2020.105926

Xiao, W. H., Shen, M. Y., Li, J. W., Li, Y. L., Qi, X., Rong, L. Y., Liu, W. M., & Xie, J. H. (2023). Preparation and characterization of curcumin-loaded debranched starch/Mesona chinensis polysaccharide microcapsules: Loading levels and *in vitro* release. *Food Hydrocolloids, 141*, 108697. https://doi.org/10.1016/j.foodhyd.2023.108697

Xing, J. J., Liu, Y., Li, D., Wang, L. J., & Adhikari, B. (2017). Heat-moisture treatment and acid hydrolysis of corn starch in different sequences. *LWT-Food Science and Technology, 79*, 11–20. https://doi.org/10.1016/j.lwt.2016.12.055

Xu, H., Ma, Q. H., Qiu, C., Wang, J. P., Jin, Z. Y., & Hu, Y. (2024). Encapsulation and controlled delivery of curcumin by self-assembled cyclodextrin succinate/chitosan nanoparticles. *Food Hydrocolloids, 157*, 110465. https://doi.org/10.1016/j.foodhyd.2024.110465

Ye, F., Miao, M., Jiang, B., Campanella, O. H., Jin, Z. Y., & Zhang, T. (2017). Elucidation of stabilizing oil-in-water Pickering emulsion with different modified maize starch-based nanoparticles. *Food Chemistry, 229*, 152–158. https://doi.org/10.1016/j.foodchem.2017.02.062

Yang, S. F., Dai, L., Sun, C. X., & Gao, Y. X. (2018). Characterization of curcumin loaded gliadin-lecithin composite nanoparticles fabricated by antisolvent precipitation in different blending sequences. *Food Hydrocolloids, 85*, 185–194.

https://doi.org/10.1016/j.foodhyd.2018.07.015

Ye, J. P., Luo, S. J., Huang, A., Chen, J., Liu, C. M., & McClements, D. J. (2019). Synthesis and characterization of citric acid esterified rice starch by reactive extrusion: A new method of producing resistant starch. *Food Hydrocolloids, 92,* 135–142. https://doi.org/10.1016/j.foodhyd.2019.01.064

Yan, X. D., McClements, D. J., Luo, S. J., Liu, C. M., & Ye, J. P. (2024). Recent advances in the impact of gelatinization degree on starch: Structure, properties and applications. *Carbohydrate Polymers, 340*, 122273. https://doi.org/10.1016/j.carbpol.2024.122273

Zou, L. Q., Zheng, B. J., Zhang, R. J., Zhang, Z. P., Liu, W., Liu, C. M., Xiao, H., & McClements, D. J. (2016). Food-grade nanoparticles for encapsulation, protection and delivery of curcumin: comparison of lipid, protein, and phospholipid nanoparticles under simulated gastrointestinal conditions. *RSC Advances, 6,* 3126-3136. https://doi.org/10.1039/C5RA22834D

Zhong, C. P., Luo, S. J., Xiong, R. Y., Liu, C. M., & Ye, J. P. (2024). A new green self-assembly strategy for preparing curcumin-loaded starch nanoparticles based on natural deep eutectic solvent: Development, characterization and stability. *Food Hydrocolloids, 151*, 109878. https://doi.org/10.1016/j.foodhyd.2024.109878

Zembyla, M., Murray, B. S., & Sarkar, A. (2020). Water-in-oil emulsions stabilized by surfactants, biopolymers and/or particles: a review. *Trends in Food Science & Technology, 104*, 49–59. https://doi.org/10.1016/j.tifs.2020.07.028

Zhang, Y., Wang, Y. M., Yang, B. J., Han, X. Z., He, Y. T., Wang, T. G., Sun, X., & Zhao, J.

(2023). Effects of zucchini polysaccharide on pasting, rheology, structural properties and *in vitro* digestibility of potato starch. *International Journal of Biological Macromolecules, 253*, 127077. https://doi.org/10.1016/j.ijbiomac.2023.127077

Zeng, X. X., Zheng, B., Xiao, G. S., & Chen, L. (2022). Synergistic effect of extrusion and polyphenol molecular interaction on the short/long-term retrogradation properties of chestnut starch. *Carbohydrate Polymers*, *276*, 118731. https://doi.org/10.1016/j.carbpol.2021.118731

Zhi, K. K., Yang, H. L., Shan, Z. G., Huang, K. R., Zhang, M., & Xia, X. D. (2021). Dual-modified starch nanospheres encapsulated with curcumin by self-assembly: Structure, physicochemical properties and anti-inflammatory activity. *International Journal of Biological Macromolecules, 191*, 305–314. https://doi.org/10.1016/j.ijbiomac.2021.09.117

Zargar, A. N., & Srivastava, P. (2024). Chapter 19 - Biosurfactants: sustainable alternatives to chemical surfactants. In R. Aslam, J. Aslam, & C. M. Hussain (Eds.), *Industrial Applications of Biosurfactants and Microorganisms* (pp. 425–436). Academic Press. https://doi.org/10.1016/B978-0-443- 13288-9.00015-2

Zhu, S. S., Qiu, Z. C., Qiao, X. G., Waterhouse, G. I. N., Zhu, W. Q., Zhao, W. T., He, Q. X., & Zheng, Z. Z. (2023). Creating burdock polysaccharide-oleanolic acid-ursolic acid nanoparticles to deliver enhanced anti-inflammatory effects: fabrication, structural characterization and property evaluation. *Food Science and Human Wellness, 12*(2), 454–466. https://doi.org/10.1016/j.fshw.2022.07.047

Zhang, B., Long, S., Feng, R., Yu, M. J., Xu, B. C., & Tao, H. (2025). Thiolated dextrin

nanoparticles for curcumin delivery: Stability, in vitro release, and binding mechanism. *Food Chemistry, 463*, 141501. https://doi.org/10.1016/j.foodchem.2024.141501

Declaration of interests

The authors declare that they have no known competing financial interests or personal relationships that could have appeared to influence the work reported in this paper.

Graphical abstract